Quiet time observations of the open-closed boundary prior to the CIR-induced storm of 9 August 2008

Kevin D. Urban,[1] Andrew J. Gerrard,[1] Yajnavalkya Bhattacharya,[1] Aaron J. Ridley,[2] Louis J. Lanzerotti,[1] and Allan T. Weatherwax[3]

[1] The open-closed magnetic field line boundary (OCB) is an important indicator of magnetospheric dynamics and can be used to identify locations of particle precipitation at the edge of the magnetosphere. The OCB can fluctuate during geomagnetic events, and the extent of this variability is a vital component of space weather research and modeling. There was a unique opportunity to identify and study the synoptic variability of the OCB during the extended 2007–2009 solar quiet period through use of the Polar Experiment Network for Geophysical Upper-atmosphere Investigations–Automatic Geophysical Observatory (PENGUIn-AGO) network of ground-based fluxgate magnetometers on the Antarctic continent. The fluxgates, which measured the occurrence of standing Pc5 modes on closed field magnetic field lines, allowed for identification of the OCB structure and study of the synoptic behavior of the OCB before and during a corotating interaction region (CIR)-driven magnetic storm. Observations were compared with results from the BATSRUS space weather model and show 83% agreement for over ~2 days before the CIR event. It is shown that such synoptic magnetometer data sets of the OCB during these storms allow for a careful test of current space weather models. The current study investigates the pre–storm time period, while a future paper will address the storm time evolution of the OCB.

Citation: Urban, K. D., A. J. Gerrard, Y. Bhattacharya, A. J. Ridley, L. J. Lanzerotti, and A. T. Weatherwax (2011), Quiet time observations of the open-closed boundary prior to the CIR-induced storm of 9 August 2008, *Space Weather*, *9*, S11001, doi:10.1029/2011SW000688.

1. Introduction

[2] The acquisition of synoptic-scale, quasi-continuous data that can used to infer the magnetic field open-closed boundary (OCB) and its morphology can have numerous uses in our understanding of magnetospheric physics and our diagnostic and prognostic numerical modeling of space weather events. For example, synoptic observations of the OCB can provide empirical forecasting models with an enhanced ability to predict substorm activity through tracking the expansion of the OCB toward the equator, which is a marker of the substorm growth phase [*Kamide et al.*, 1999; *Milan et al.*, 2003]. In addition, all current space weather models need to be initialized with data that is typically obtained from a diagnostic data assimilation scheme (e.g., Center for Space Environment Modeling Space Weather Modeling Framework, Center for Integrated

Space Weather WSA-ENLIL Operational Model). More advanced forecasting models can also ingest additional real-time data (i.e., continuously obtained and site specific) to better constrain (i.e., "nudge") real-time model runs (e.g., Air Force C/NOFS modeling system).

[3] More practically, the identification of the OCB can be used to identify spatial regions prone to solar particle events (SPEs) and/or polar cap absorption (PCA) patches. The effects of SPEs are deleterious to spacecraft, astronaut safety, passengers on board high-altitude aircraft, and—to a lesser extent—passengers on board commercial aircraft [*Shea and Smart*, 1998; *Jones et al.*, 2004]. PCA events can disrupt HF radio communications and can cause radio black out for potentially several hours or longer [*Rose and Ziauddin*, 1962; *Patterson et al.*, 2001].

[4] In this paper we show that a strategically designed high-latitude network of fluxgate magnetometers can provide nearly continuous, real-time, synoptic data on the state of the OCB. Specifically, data from a network of fluxgate magnetometers—deployed as part of the Polar Experiment Network for Geophysical Upper-atmosphere Investigations (PENGUIn) program—has been used to

---

[1]Center for Solar-Terrestrial Research, New Jersey Institute of Technology, Newark, New Jersey, USA.
[2]University of Michigan, Ann Arbor, Michigan, USA.
[3]Department of Physics, Siena College, Loudonville, New York, USA.
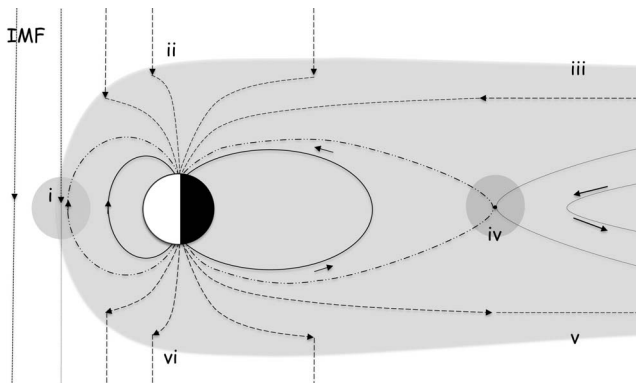

Figure 1. The magnetosphere (XZ plane, GSM coordinates). Region i represents the dayside merging of geomagnetic field lines with interplanetary magnetic field. The open closed boundary—the frontier set of open field lines—originates in this region. As the solar wind drags the IMF past the Earth, the newly connected field lines exhibit a i–ii–iii motion; the field lines are dragged deep into the tail, ultimately undergoing a reconnection process again in region iv. Dotted lines refer to the IMF before interaction with the magnetosphere, while solid lines correspond to closed geomagnetic field lines. The dot-dot-dashed lines correspond to the OCB, while all the long-dashed lines in between represent open (reconnected) field lines.

infer the location of the OCB by their ability to detect Pc5-type waves on closed magnetic field lines. Herein we demonstrate the capabilities of such a network of magnetometers to monitor the OCB during a period of low solar and geomagnetic activity in early August 2008 preceding a moderate corotating interaction region (CIR [e.g., *Tsurutani et al.*, 2006; *Riley*, 2007]) event. We discuss the fluxgate measurements in detail, describe the process of how the OCB location is determined, and then compare our OCB results to those predicted by the Block Adaptive-Tree Solar-wind Roe-type Upwind Scheme (BATSRUS) model. Ultimately, we demonstrate the possibility of implementing a real-time OCB automatic detection scheme that could be used to enhance space weather forecasts. A future paper will continue the analysis for the period immediately following characterized by the CIR event.

2. OCB Diagnostics and Determination

[5] The reconnection rates at the dayside magnetopause and in the magnetotail are commonly used in determining the state of the magnetosphere. The polar cap inflation/deflation model introduced by *Siscoe and Huang* [1985] demonstrated that the size of the polar cap is intimately associated with the reconnection rates on the dayside and nightside. If the polar cap area can be estimated, along with its time rate of change, then one can deduce the difference in dayside/nightside reconnection rates. That is, expansion of the polar cap indicates that the dayside creation of open

flux at the magnetopause is outperforming the destruction of open flux in the nightside magnetotail. Observed decreases in area (contractions) imply the opposite scenario. Computations of this type are important since, for example, estimations of the dayside reconnection provide a measure on how much energy, momentum, and mass is currently loading into the magnetosphere-ionosphere system from the solar wind.

[6] The area of the polar cap has also been shown to be a reasonable indicator of the amount of energy currently stored in the magnetotail available for substorms and that the variation in the polar cap's size and shape is closely associated with substorm phases, although different conclusions have sometimes been reached [e.g., *Kamide et al.*, 1999; *Brittnacher et al.*, 1999]. Studies of *Milan et al.* [2003] and *Lockwood et al.* [2005] discuss the relationship between the dayside polar cap boundary and substorm phase, and *Milan* [2004] discusses energy storage in the magnetotail and its relation to polar cap size.

[7] As such, a large number of studies have been dedicated to estimating the variation of the polar cap boundary, referred to herein as the OCB. In line with the given definition of the polar cap, the OCB is the separatrix between the magnetosphere's open field lines which reconnect with the interplanetary magnetic field (IMF), and the closed field lines which form a closed loop (Figure 1). Since it is often impractical to monitor the location and motion of the entire OCB at all local times for various experimental reasons, most studies strive to approximate the boundary by monitoring a limited portion and then employing an interpolation method. Given a reasonable approximation of the OCB over time, the polar cap area (and its rate of change) can be estimated and then, using a model such as that of *Siscoe and Huang* [1985], the total open flux content of the magnetosphere as well as the difference in dayside/nightside reconnection rates can be deduced.

[8] However, the issue of "what constitutes a reasonable approximation of the OCB" is a contested issue. For example, many studies have employed a single data point obtained from a polar-crossing satellite to estimate the OCB as a circular structure as a coarse first-approximation of the realistic shape. *Sotirelis et al.* [1998] attempted to study the shape of the OCB using four DMSP satellites to validate whether a single data point provided a reasonable approximation of the OCB. They showed that the variability of the size, shape, and location of the OCB was extensive enough to disqualify simplifying assumptions, such as single data-point circular approximations. They recommended that 3–4 data points gathered within the span of an hour be used for acceptable cubic spline approximations of the OCB. Furthermore, higher temporal or spatial resolution would require significantly more polar-orbiting satellites.

[9] Depending on the level of detail desired, significantly more data points may be required; a reasonable approximation for one study may be grossly underestimated in another. For example, studies interested in an estimate of the polar cap area obviously require less data points than

studies that require a detailed account of the variation of the polar cap over all local times. Knowledge of only the size of the polar cap inherently contains no site-specific information and thus is not useful in determining how the OCB varies azimuthally for a prescribed set of space weather parameters. Such precise site-specific information is crucial to many ongoing areas of research which include the investigation of reconnection rates at the magnetopause [*Lockwood et al.*, 2005] and in the magnetotail [*Milan*, 2004], analyzing how the OCB synoptically transforms throughout the substorm cycle, and modeling the magnetospheric system more accurately [*Tsyganenko*, 1995; *Pulkkinen and Tsyganenko*, 1996; *Rae et al.*, 2004; *Gombosi et al.*, 2004].

[10] To obtain detailed information concerning the OCB's motion and location, system-wide monitoring of the OCB must be implemented, which often includes the utilization of a diverse assortment of instruments and analysis techniques [e.g., *Lessard et al.*, 2009]. Particle precipitation measurements, for example, are deemed by many authors to be a satisfactory method for field line identification and satellites are a great way of obtaining in situ measurements, but this method of OCB identification can be impractical as a stand-alone for synoptic-scale studies. Furthermore, *Oksavik et al.* [2000] showed incongruities in two sets of satellite measurements, suggesting the possibility that polar passes do not have a good enough resolution to accurately determine if a field line is open or closed. Many other methods for determining the location of the OCB have been studied. *Rodger* [2000] discusses various ground-based attempts at monitoring the OCB. *Milan et al.* [2006] describes both ground- and space-based techniques; for example the "trapping boundary" (poleward edge of high energy electron precipitation characteristic of closed field lines) can be used as a primary proxy of the dayside OCB, and the edge between polar rain and the harder precipitation associated with discrete aurora can be exploited as a nightside OCB proxy. *Moen et al.* [2004] found that VHF radar measurements can be used to study the dayside OCB.

[11] Many researchers have established OCB detection techniques in a wide range of magnetic local time (MLT) from analysis of data obtained from the Super Dual Auroral Radar Network (SuperDARN). This is often done by identifying the spectral width boundary (SWB) found in the radar data with the OCB. For example, *Baker et al.* [1995] showed the SWB to be a viable proxy for the OCB in the cusp region ionosphere, while *Chisham et al.* [2004] established this proxy for the midnight sector (~1800–0200 MLT). *Chisham et al.* [2005a] conclude that although the SWB approximates the OCB well near midnight and times before noon (~0800–1200 MLT), it cannot be reliably employed as a proxy in the early morning MLT region (~0200–0800 MLT). It has been shown by *Chisham et al.* [2005b] that SWBs found in the afternoon sector are only reliable OCB proxies for geomagnetic latitudes greater than ~74°.

[12] Monitoring the OCB using a high-latitude network of fluxgate magnetometers can greatly aid in synoptic-scale studies. Information obtained from such a network enables researchers to determine whether the OCB is within, out-

side, or on a particular geomagnetic latitude at a given magnetic local time, and when a transition in the OCB state occurs (e.g., from inside to outside a geomagnetic latitude). A truly synoptic-network of fluxgate magnetometers would not include the spatial-temporal resolution/distortion issues inherent in space-based measurements. Furthermore, as we show herein, magnetometer measurements are not constrained to the dayside or nightside; a magnetometer is equally suited for all MLT.

3. Instrumentation and Data Processing

[13] The PENGUIn program began as an effort to establish and maintain a network of ground-based geophysical observatories at the highest of geomagnetic latitudes. A network topology such as this ensures that observations of phenomena closely related to the plasma dynamics of the dayside magnetopause and the boundary of the magnetospheric tail are possible. To realize this goal, PENGUIn established the Automated Geophysical Observatories (AGOs). The AGOs can operate unmanned for a full year, powered by sunlight and the wind, before servicing is required [*Rosenberg and Doolittle*, 1994; *Mende et al.*, 2009]. Instruments housed within each AGO include an imaging riometer, both a searchcoil and a fluxgate magnetometer, an all-sky imager, an ELF/VLF receiver, and a LF/MF/HF receiver.

[14] AGO sites were located such that the sites form two arrays along carefully separated geomagnetic meridians. The configuration ensures that the temporal and spatial effects associated with polar cap observations can be distinguished and separated (Figure 2). One meridional array is along the geomagnetic meridian that includes South Pole Station (SPA) and stretches from the latitude of the polar cusp (approximately 70° geomagnetic latitude under highly disturbed conditions) to the pole of the dipole magnetic field. This array consists of sites P2, SPA, P1, and P5. The second array is positioned approximately 1.6 hours earlier in MLT and consists of the AGOs sites P3, P4, P5, and P6.

[15] Magnetometer data used in this study were available from SPA, McMurdo (MCM), and AGOs locations P2 and P3 (Table 1). These sites often pass through the OCB owing to their geomagnetic latitude, which is ideal for a synoptic-scale determination of the OCB. We note that P1 was operational during 2008, but there were data dropouts in the early August period. Data from P4, P5, and P6 were all offline during the austral winter of 2008. The three-axis fluxgate magnetometers at SPA, MCM, and the AGO sites measured the relative variation of the geomagnetic field at 1-second sampling intervals with an accuracy of 0.01-nT. Data for all three axes of the fluxgate magnetometers were analyzed, but only the H-component (i.e., the north-south field line component) is discussed herein.

[16] To create uniform 10-sec data realizations, the raw 1-second fluxgate data samples from each site were averaged and resampled into independent 10-second intervals, thus accounting for any individual missing data records or other issues associated with the remote data acquisition
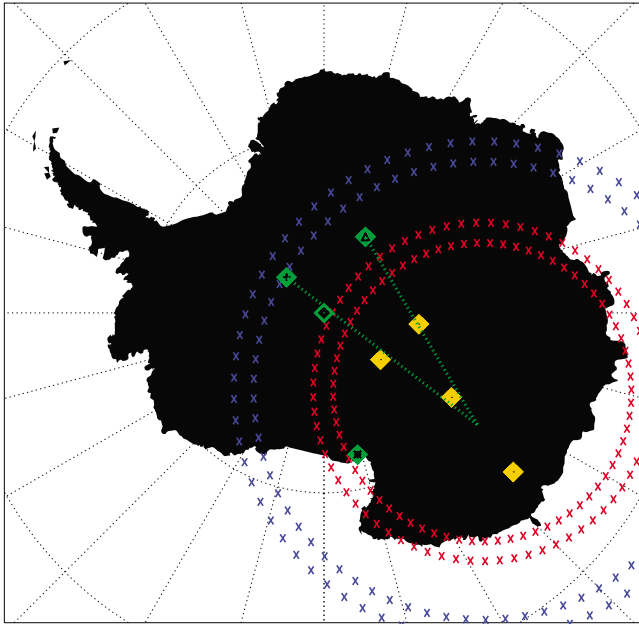
Figure 2. Locations of data sites used in this study. SPA (black diamond on green diamond), MCM (black asterisk on green diamond), P2 (black plus sign on green diamond), and P3 (black triangle on green diamond) are shown in geographic coordinates with 0° longitude pointing to the top. Yellow diamonds show the location of the other PENGUIn-AGO sites that did not record data during this period due to power issues. The green dashed lines approximate geomagnetic meridians stemming from the geomagnetic pole. The purple cross regions represent the location of the equatorward side and the poleward side of the auroral boundary for each geomagnetic longitude at 0000 magnetic local time during low solar activity (Ap less than 30). The red cross regions represent the location of the equatorward side and the poleward side of the auroral boundary for each geomagnetic longitude at 1200 magnetic local time during low solar activity, as determined by *Holzworth and Meng* [1975]. These zones expand during high solar activity.

system. This data series was then high-pass filtered to create a zero-mean sequence and to remove periods longer than 2-hours. A running Hanning window of 1-hour duration, stepped forward in time every 10-mins, was then used to compute an estimate of the power spectral density

(PSD) as a function of time (Figure 3 (top) shows one particular PSD estimate). To better identify features within each PSD estimate, each spectrum was transferred to the log-log domain (Figure 3, middle) where a linear fit spanning the frequency spectrum was estimated and then subtracted, leaving behind the PSD residual (Figure 3, bottom), i.e., much like that used by *Lanzerotti et al.* [1999] and *Gerrard et al.* [2010]. The time series of the PSD residuals for the four data locations, obtained between 1 and 12 August 2008 and used in this study are shown in Figure 4.

4. Observations

[17] In the time-series of residual PSD estimates, two frequency bands are relevant to our study: those having periods between three and nine minutes, known as Pc5 modes, and those with periods greater than ten minutes, which we will call long-period (LP) modes. High power in the Pc5 band corresponds to the frequencies of standing Alfven waves on a closed field line [*Lanzerotti et al.*, 1999; *Lessard et al.*, 2009]. Isolated Pc5 presence (that is, Pc5 power without simultaneous power in the LP band) generally appears to coincide with closed field lines on the dayside (although exceptions exist as discussed below). LP modes are only sparsely detected on the dayside and are typically associated with extended field lines stretching into the magnetotail. These extended field lines can either be closed or open. When high power is registered in both the Pc5 and long-period bands, it is very likely a closed magnetotail field line being sampled; isolated LP presence is not so clear. When there is a lack of power in both the Pc5 and LP bands, we interpret this as sampling an open field line, although there exist the possibility, for example, that a closed field line without associated Pc5 modes can be mistaken for an open field line. However, it is likely there is always energy available on the dayside to drive field line resonances (e.g., from sources such as the Kelvin-Helmholtz instability along the magnetopause and waves in the solar wind). Although it is a bit more questionable whether or not energy availability is as persistent on the nightside, this is also likely the case since processes that produce the aurora are active even during quiet times. Thus, analysis of power in each of these frequency bands indicates the type of magnetic field line, and synoptic analysis allows for an estimation of the actual OCB.

[18] Indeed, the 1–6 August power spectra at SPA (Figure 5) demonstrate this repeated 24-hour periodicity of Pc5 and LP structure. Given that during an extended interval of geomagnetic quiescence in which SPA generally

Table 1. Magnetometer Locations

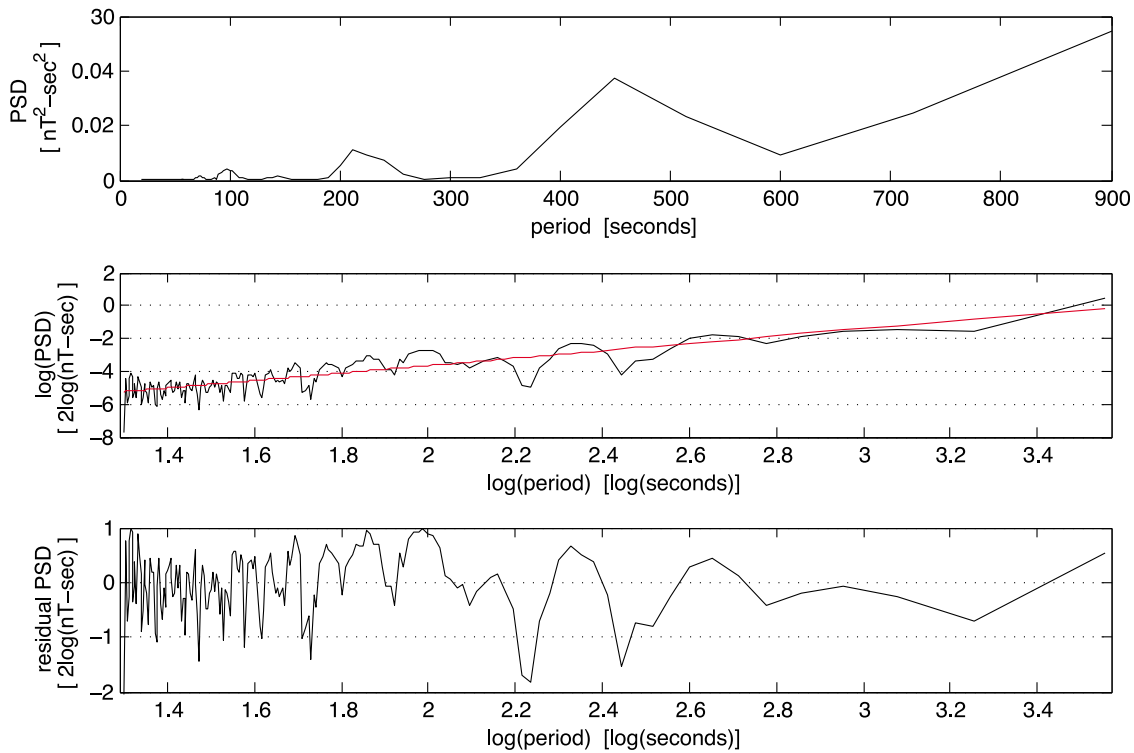| AGO/Station	Geographic Latitude	Geographic Longitude	CGM Latitude	CGM Longitude	Local Noon
P2	S 85.67	E 313.62	S 69.84	E 19.33	15:29
P3	S 82.75	E 28.59	S 71.80	E 40.25	14:02
MCM	S 77.85	E 166.67	S 79.94	E 326.97	18:57
SPA	S 90.00	E 000.00	S 74.02	E 18.35	15:35

Figure 3. The power spectra times series was created from the H-component data traces using a 1 h Hanning window incremented forward in time in 10 min steps. (top) An example of the initial power spectra produced from a 1 h window. (middle) To better visualize dynamic range of the PSD it is rendered in the log-log domain. (bottom) A best fit line to the log-log data was subtracted from the PSD, leaving the "residual PSD."

crosses under the OCB at least twice per day (also shown in Figure 2, based on *Holzworth and Meng* [1975]), one would expect to see examples of both open and closed field lines as described above. This is also seen in the individual day analyses given for SPA in Figure 5. Looking at any particular geomagnetically quiescent day (3, 4, 7, and 8 August being most distinct), one can identify the form of a swooping "U-shape" in the residual power spectra during a 24-hour period. For the most part, nightside measurements generally have high-power in both bands—measurements indicative of closed magnetotail field lines—although there occasionally exists the presence of LP modes without simultaneous Pc5s. Open field lines can be also identified, albeit sparsely, on the nightside by the lack of both bands (e.g., 7 and 8 August in Figure 5).

[19] A transition (occurring in the dawn sector) can be identified in the power spectra as the first half of a swooping "U" shape (easily discernible in the day plots); this transition in the power spectra, during quiet time, often corresponds to the fluxgate transitioning from night to day. This transition is observed as a shift from field lines exhibiting both Pc5 and LP modes (closed magnetotail field lines) to field lines exhibiting only Pc5 modes (closed dayside modes). Going forward in time, another distinct transition is seen, completing the "U" shape. This transition is

often seen to be from an extended interval of isolated Pc5 modes (resonances on closed dayside field lines) to simultaneous power in both frequency bands (closed magnetotail field lines) and roughly corresponds to the fluxgate transitioning from the dayside to the nightside, although on 8 August (Figure 5) this transition happened unusually early (in a future paper we will show that this corresponds to the approach of a corotating interaction region).

[20] Referring to Figure 1, the "U" shape can be interpreted as follows: Since typical nightside measurements exhibit power in both the Pc5 and LP bands, occasionally losing Pc5 power, the associated field lines exist within the iv–v region or earthward of iv; isolated Pc5 modes found on the dayside coincide with field lines earthward of the magnetopause (region i).

[21] It is evident in the SPA records that there can exist extended intervals of open field lines at times surrounding local noon. This feature in the data suggests that a protrusion, or nub, extending from the sunward base of the approximately pear-like OCB. *Sotirelis et al.* [1998] have a figure that demonstrates this shape. In addition, *Birn et al.* [1991] show that the OCB during quiet time is roughly shaped like an arrowhead pointing sunward.

[22] AGO stations P2 and P3 are approximately at the same geomagnetic latitude (separated in MLT by 1 h 27 m)
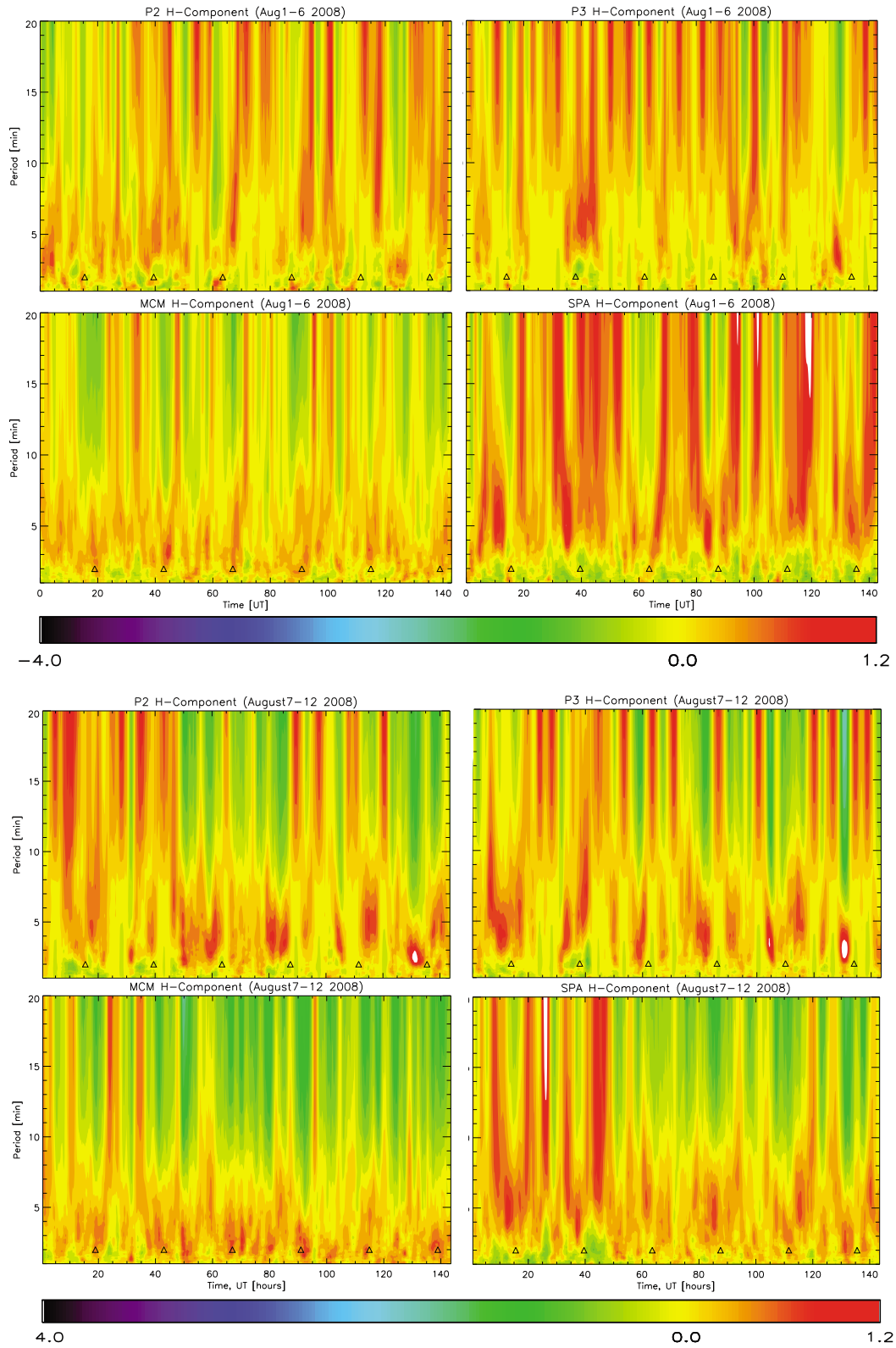
Figure 4

and can be expected to exhibit similar, slightly time-offset behavior. From Figure 4, it is clear both fluxgates register closely resembling Pc5 and long-period behavior.

[23] By directly comparing P2 and SPA data (Figure 6), which are approximately on the same geomagnetic longitude, such a latitudinal dependence can be better investigated. Closely corresponding structure can be found between P2 and SPA. However, the residual power across both frequency bands is lower at P2 as compared to SPA. Study of Figure 3 shows that residual power at P3 and MCM is also weaker as compared to SPA, with MCM being much weaker than all other sites. This indicates that the residual power increases with geomagnetic latitude until the OCB is reached, at which point the residual power drops dramatically as open field lines are encountered (e.g., MCM is approximately within the OCB at nearly all times). The relative scarcity of power throughout the entire frequency range over the quiet period (Figure 4) clearly illustrates that MCM, in general, fails to register a substantial amount of closed field lines of any sort (dayside or nightside). However, a low-power Pc5 structure persists—a phenomenon that is commented on later.

5. Determination of the OCB and Comparisons to the BATSRUS Model

[24] In an effort to implement an automatic OCB detection scheme, the PSD residuals for the H-components at each site were integrated in the 3- to 9-min periodicity band corresponding to Pc5 oscillations and in the 10- to 30-min periodicity band corresponding to tail oscillations. The integrated power was then weighted by the inverse sine of the geomagnetic latitude (i.e., $1/\sin(\phi)$ term) to account for the approximately spherical divergence of the field lines. These spectral data form a relative measure of the power in the Pc5 band (i.e., closed field lines) and the deeper tail band (i.e., extended field lines) for each site. The integrated spectra in both bands from 7–12 August are shown in Figure 7; a period chosen to contain no geomagnetic activity (7 and 8 August, which are similar to data from 1 to 6 August and not shown) and CIR-induced activity (9–12 August).

[25] As discussed in the previous section, because MCM is generally located within the polar cap on open field lines

for all MLT during low solar activity, we can use the integrated fluxgate spectral data from that site as a baseline measure of activity. Hence, we don't expect greater Pc5 activity from MCM data as compared to other sites; the MCM values can thus be used to set a detection threshold. If a particular site has more power in the Pc5 band than this threshold, then we flag the site as existing on a closed field line. Similar reasoning has been applied to determine the threshold for the long power bands using MCM as a baseline. However, we note that in the latter case (long-period band) the assumption is not as robust: over the course of 24-hours, MCM is sometimes near the OCB and can actually exist under a deep tail field line.

[26] Having determined these thresholds, four categories emerge, three of which correspond to a closed field line event (i.e., the sampling of a closed field line) and one of which corresponds to an open field line event. The three categories that qualify as a closed field line event are as follows: (1) high power in the Pc5 band and low power in the long-period band) where "high" and "low" are determined by the thresholding conditions); the site is flagged as being on a closed field line. (2) Low power in the Pc5 band and high power in the long-period band; the site is flagged as being on a closed field line that is likely extended into the deep tail region. (3) High power in both the Pc5 band and the long-period band; the site is flagged as being on a closed field line likely extending into the relatively near-Earth tail region. An open field line event corresponds to the remaining condition: when there exists low power in both the Pc5 band and the long-period band. It is only when this condition is met that the site is flagged as being on an open field line. Synoptic inspection of the field line maps from all the sites (e.g., P2, P3, SPA, and MCM in this study) allows one to identify the location of the OCB. The accuracy with which this can be done is determined by the spatial separation distance between the sites, similar to how synoptic data assimilation is ingested in tropospheric weather models.

[27] To validate the methodology of OCB determination thus developed, we compared our observational results with predictions of the OCB by the BATSRUS numerical model which was coupled with an ionospheric electrodynamics solver [*Ridley et al.*, 2004] throughout the 7–

Figure 4. Time series spectrograms of the residual PSD, as determined by the H-axis fluxgate magnetometer measurements, for each site used in this study from 1–6 August 2008 (top set of four, time is hours since 0000 UT of 1 August) and 7–12 August 2008 (bottom set of four, time is hours since 0000 UT of 7 August). Triangles denote magnetic noon at each of the sites. The data span a factor of 180 in magnitude (in natural log domain) from highest to lowest on a ROYGBIV color table, respectively. High power in the Pc5 band generally coincides with a closed field line, while high power in the long-period (LP) band coincides with an elongated field line (stretching into the tail) that may or may not be closed. Four combinations of Pc5 and LP exist: (1) isolated Pc5 presence, which generally appears to coincide with closed field lines on the dayside; (2) the presence of both Pc5 and LP modes, typically found on the nightside and thought to coincide with elongated, closed field line stretching into the magnetotail; (3) isolated long-period modes, sometimes characteristic of the nightside and thought to coincide with extremely elongated magnetotail lines that may or may not be closed; and (4) the lack of both Pc5 and long-period modes, which generally coincides with an open field line (although the possibility exists, for example, that a closed field line without associated Pc5 modes can be mistaken for an open field line).
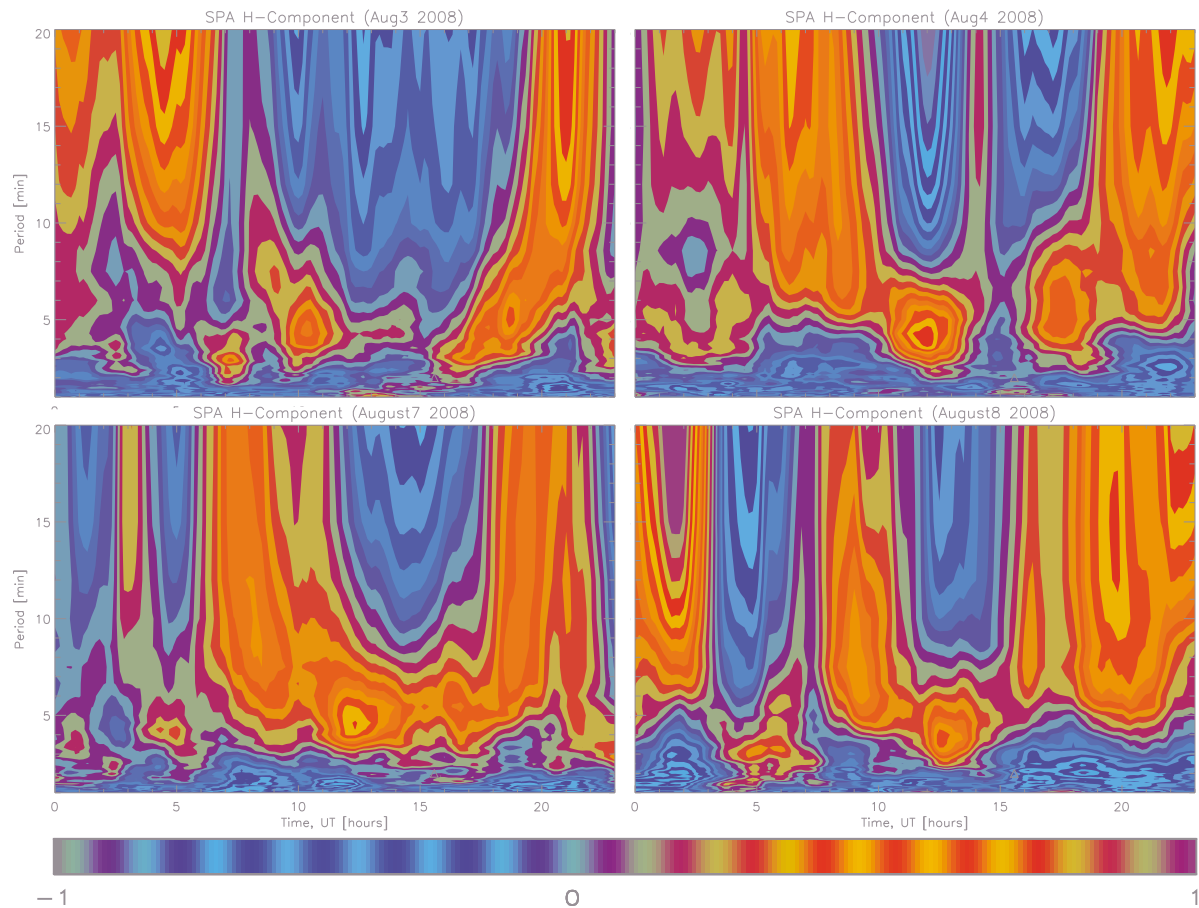
Figure 5. Closeup of residual PSDs from SPA. The selected coloring emphasizes the residual power structure in the H-component fluxgate magnetometer measurements during the relatively quiet period on select August 2008 days. The typical quiet time residual power pattern has a characteristic swooping "U" shape in the long-period band (frequencies along elongated field lines), marking a clear diurnal variation. From these plots it is seen that a typical quiet time residual power signature during an interval on the nightside includes both long-period and Pc5 modes, whereas a typical interval on the dayside includes mostly Pc5 modes.
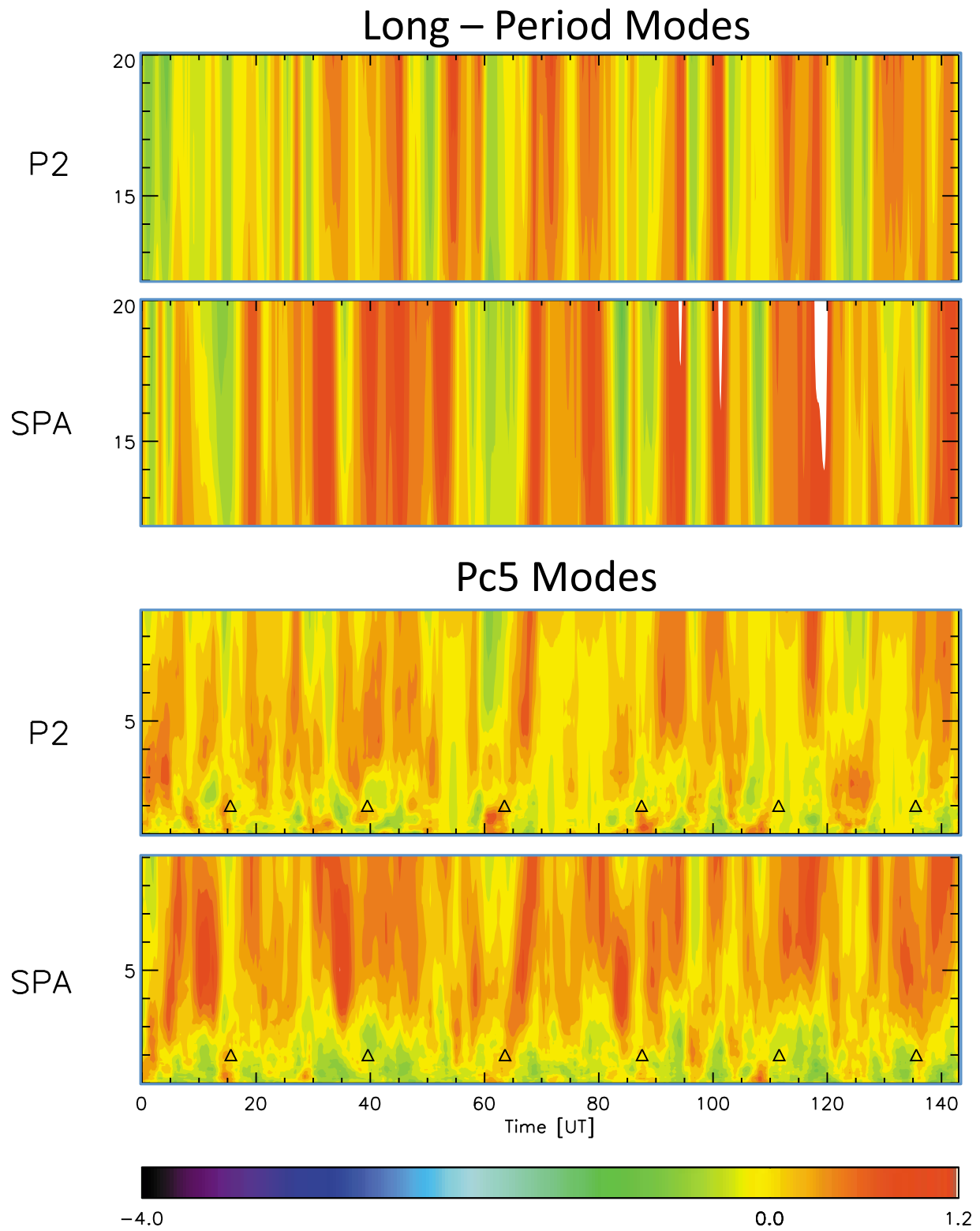
Figure 6. Comparison of data from P2 and SPA in long-period and Pc5 bands. Time is hours since 0000 UT of 1 August. The vertical scale denotes periodicity in minutes. Triangles denote magnetic noon at each of the sites. The data span a factor of 180 in magnitude (in natural log domain) from highest to lowest on a ROYGBIV color table, respectively.
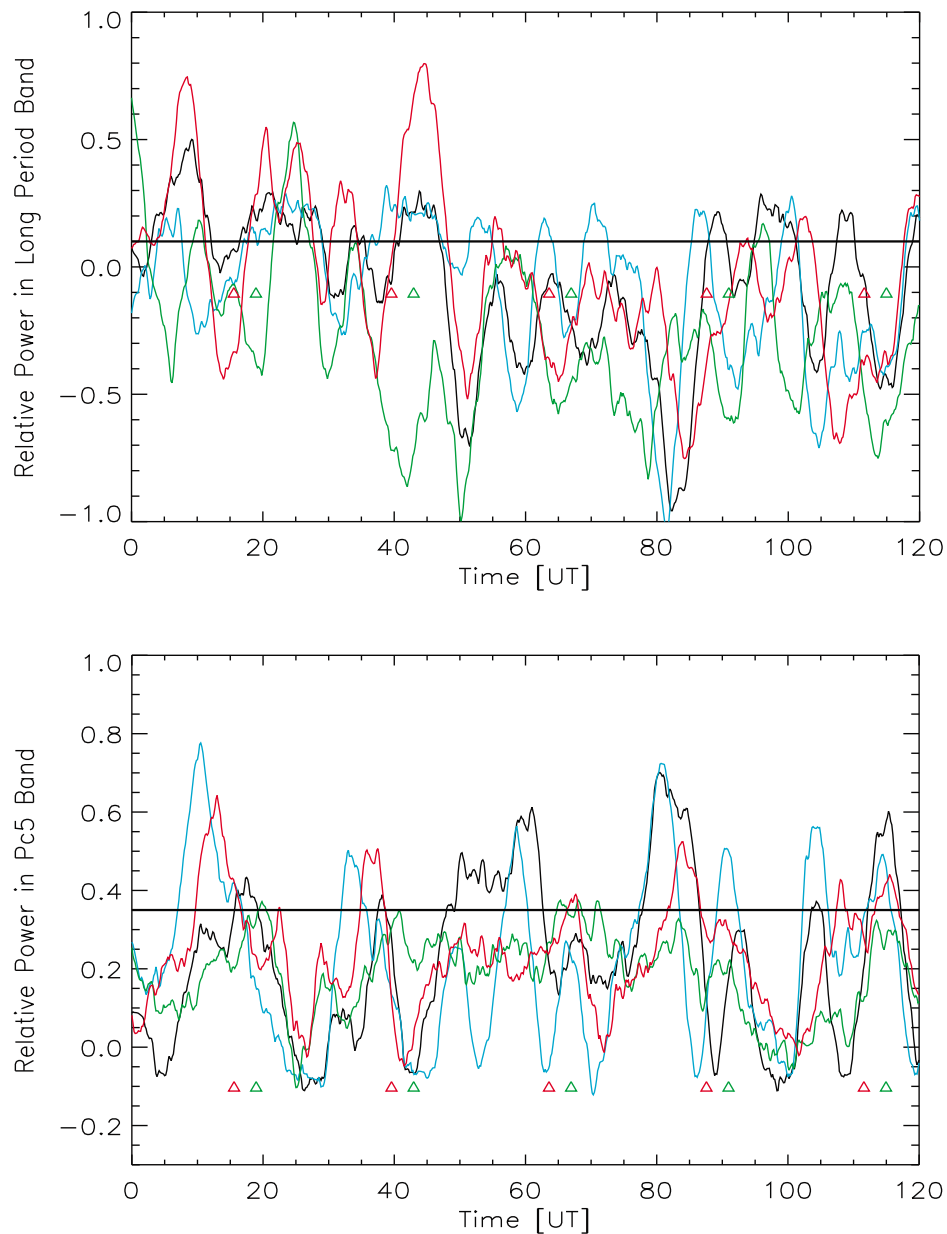
Figure 7. Time series of the integrated residual PSDs for each of the four sites (SPA, red; MCM, green; P2, blue; and P3, black) in the (top) long-period band and (bottom) Pc5 band. The data thresholds used herein are indicated by the horizontal black line on each plot. Time is hours since 0000 UT of 7 August. Triangles denote magnetic noon at SPA (red) and MCM (green).

11 August time period—an interval that was temporally limited for computational reasons yet, as mentioned above, still included a quiet period (7–9 August) and a CIR period (9–11 August). This particular model was chosen because its predictions of the OCB have been shown to be in good agreement with photometer observations of the OCB during quiet, steady conditions [*Rae et al.*, 2004]. The BATSRUS model utilizes the magnetohydrodynamic equations to study a range of plasma phenomena, including the interaction of the solar wind with planetary magnetospheres

[*Gombosi et al.*, 2004; *Toth et al.*, 2005]. For this run, the output of the modeled OCB was acquired every 1-hour for the 5 days studied, requiring 10 computational days to process (and thus the reason for the choice of the 5-day span of 7–11 August). A sampling of results for the 7–8 August period (i.e., the quiet time period) are shown in Figure 8.

[28] The prediction of the OCB from the fluxgate measurements, taken on the same 1-hour time steps as the model results, matched the modeled OCB 83% of the time during this quiet geomagnetic period spanning ~58 hours,
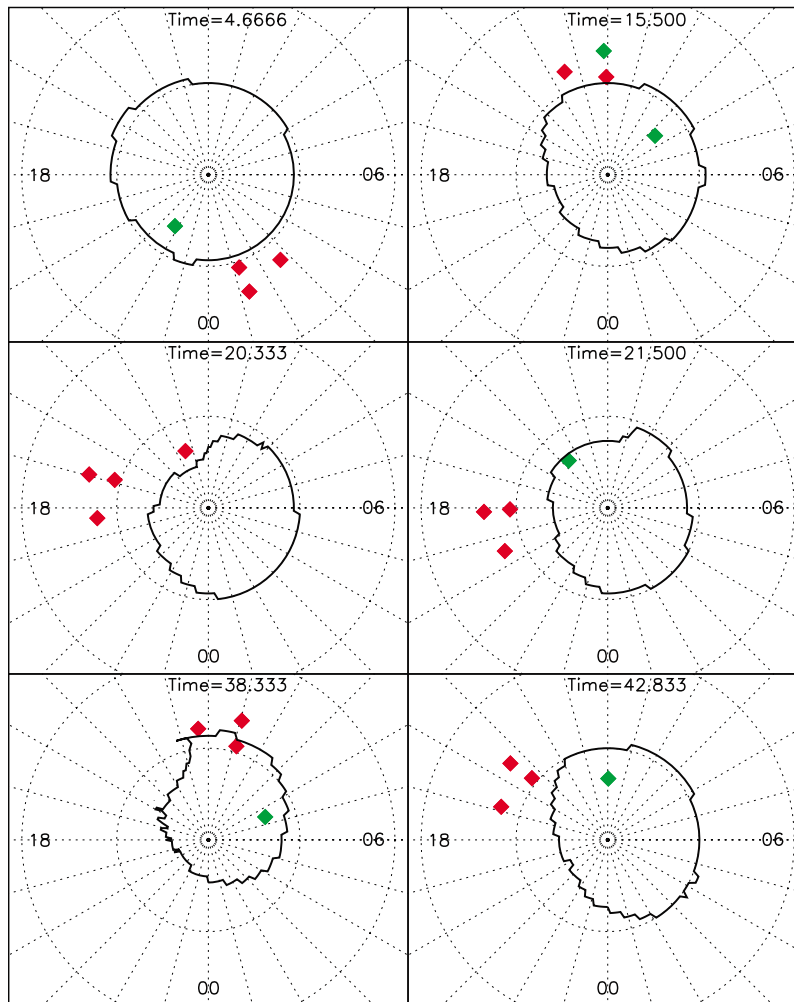
Figure 8. Sample comparison of field lines as determined by the four fluxgates (data points) with the modeled OCB as determined by the BATSRUS model (thick boundary). Green points indicate an open field line, while red points indicate a closed field line. Magnetic noon is toward the top of the sheet. Time is UT hours since 0000 UT of 7 August.

indicating that the technique is quite viable to obtain the OCB in real-time determinations. Based on a reduced chi-square test, the probability of obtaining this agreement with a random sampling of points is much less than 1%, indicating that the data and model are showing a statistically significant relationship. Instances when the fluxgate determination of the OCB didn't match the modeled OCB came in two varieties: (1) Either the fluxgates gave inconsistent results making identification of the OCB impossible (e.g., at t = 15.500 hours of Figure 8), or (2) when a fluxgate does not agree with the OCB determined by the model (e.g., at t = 38.333 hours of Figure 8).

6. Discussions and Conclusions

[29] On the basis of previous work [*Lanzerotti et al.*, 1999] and having shown that observations largely agree (~83%)

with output of the BATSRUS global magnetospheric model (previously established to accurately represent the OCB during quiet geomagnetic conditions [*Rae et al.*, 2004]), we conclude that real-time determination of the OCB can be successfully accomplished with reasonable accuracy using an array of fluxgate magnetometers, as was demonstrated herein for the period 1–9 August 2008, using the PENGUIn-AGO array of fluxgate magnetometer instruments. The steady, repeatable features at the four network locations (shown in Figures 4–6) follow the gross features of the OCB-polar cap environment and make it possible to make more detailed studies of this environment. For instance, analysis of small-scale features of the OCB-morphology during substorm processes may yield some significant insight into storm time dynamics.

[30] Three major considerations to the proposed methodology to determine the OCB need to be further investi-

gated. First, the thresholding level, as determined by MCM data herein, should be based on fluxgate magnetometer data from a higher geomagnetic latitude. Ideally, the PENGUIn-AGO P5 site (S 86.74 CGM), located close to the southern geomagnetic pole, would be more of an ideal reference site to use to determine this threshold level. We are currently trying to implement a real-time determination of the OCB using P5 as that reference when data are available.

[31] Second, recent observations of periodicities within the solar wind have been reported that fall into the Pc5 band [*Thomson et al.*, 1995; *Kepko et al.*, 2002; *Eriksson et al.*, 2005; *Liou et al.*, 2008]. Should these periodicities be resolved on open field lines, one may incorrectly attribute such a field line as closed and thus fail to correctly identify the OCB. Cursory examination of ACE solar wind data indicate, for example, that such periodicities were in fact present during the collection of the 1–12 August data presented here. However, we note that, assuming the Pc5-type periods are globally homogeneous over the polar region, they would only act to equally bias the residual power measured in the Pc5 band at all the sites, and thus not impact the analysis methodology presented here. Should this assumption of homogeneity fail, then the DC biasing of the residual PSD would be unequal and make determination of the threshold level much more difficult.

[32] Third, the accuracy of the OCB location and structure fundamentally depends on the geophysical locations, and thus spatial separation, of the fluxgate magnetometers being used. On the basis of what we know of the OCB morphology, such an array of instruments should be distributed approximately every 4 hours in MLT, with at least three fluxgates spanning the range of geomagnetic latitudes where the OCB is climatologically located. The array of fluxgates used herein did not cover the MLT sufficiently but can be used as a proof-of-concept nonetheless. An expanded array would allow for truly synoptic, real-time observations of the OCB at all MLT.

[33] The spatial and temporal mapping of the OCB has many practical uses. For example, in post-SPE analysis, a synoptic-scale data set of the morphological dynamics of the OCB can be utilized to enhance current estimates of radiation dosages attained by airline crews on transpolar flights. The aim of *Butikofer et al.* [2007] is to make more precise estimates of cosmic radiation exposure by taking into account the anisotropy of solar particle radiation across the globe—knowing the precise morphology of the OCB at the time of transpolar flight can further improve these estimates. In conjunction with an SPE database, precise estimates such as these can prove to be very important for frequent flyers, especially those whose travel is regularly on transpolar flights between the United States and Asia [*Barish*, 2009; *Barish and Dilchert*, 2010]. The U.S. Federal Aviation Administration has set guidelines that recommend yearly maximal cosmic radiation exposure dosages for aircrews and the general public [*Friedberg et al.*, 2000]. Better dosage estimates can better inform frequent flyers of their exposure to radiation and promote public safety, and

precise estimates may be even more important for European nations, where law currently enforces radiation exposure regulations. As another example, a very practical benefit of a real-time automatic OCB detection scheme would be to give aircraft an accurate portrayal of the polar cap structure and location. For example, in the event of an SPE, this could permit aircraft to find the safest and most optimal (i.e., cost-efficient) flight route.

[34] In a future paper we will continue our comparison of the fluxgate magnetometer measurements of the OCB with those predicted by the BATSRUS model for the 9–12 August period; a period in which geomagnetic activity was driven by a corotating interaction region (CIR) and its associated high-speed solar wind stream (HSS). To remove ambiguity concerning the validity of our observational method versus that of the model during geomagnetically active times, we will make comparisons with measurements made of the particle precipitation boundary (PPB) made by polar-orbiting spacecraft, such as DMSP satellites, and in the future will use established photometer techniques. To be thorough, other physics-based models, such as the Open Geospace General Circulation Model (OpenGGCM), and empirical models, such as those of Tsyganenko, are being looked into for comparative analysis as well.

References

Baker, K. B., J. R. Dudeney, R. A. Greenwald, M. Pinnock, P. T. Newell, A. S. Rodger, N. Mattin, and C.-I. Meng (1995), HF radar signatures of the cusp and low-latitude boundary layer, *J. Geophys. Res.*, 100, 7671, doi:10.1029/94JA01481.

Barish, R. J. (2009), Health physics and aviation: Solar cycle 23 (1996–2008), *Health Phys.*, 96(4), 456–464.

Barish, R. J., and S. Dilchert (2010), Human resource responsibilities: Frequent flyer radiation exposure, *Employee Responsibilities Rights J.*, 22(4), 361–369.

Birn, J., E. W. Hones, J. D. Craven, L. A. Frank, R. D. Elphinstone, and D. P. Stern (1991), On open and closed field line regions in Tsyganenko's field model and their possible associations with horse collar auroras, *J. Geophys. Res.*, 96(A3), 3811–3817.

Brittnacher, M., M. Fillingim, G. Parks, G. Germany, and J. Spann (1999), Polar cap area and boundary motion during substorms, *J. Geophys. Res.*, 104(A6), 12,251–12,262.

Butikofer, R., E. O. Fluckiger, L. Desorgher, and M. R. Moser (2007), The extreme solar cosmic ray particle event on 20 January 2005 and its influence on the radiation dose rate at aircraft altitude, *Sci. Total Environ.*, 391(2–3), 177–183.

Chisham, G., M. P. Freeman, and T. Sotirelis (2004), A statistical comparison of SuperDARN spectral width boundaries and DMSP particle precipitation boundaries in the nightside ionosphere, *Geophys. Res. Lett.*, 31, L02804, doi:10.1029/2003GL019074.

Chisham, G., M. P. Freeman, T. Sotirelis, R. A. Greenwald, M. Lester, and J. P. Villain (2005a), A statistical comparison of SuperDARN spectral width boundaries and DMSP particle precipitation boundaries in the morning sector ionosphere, *Ann. Geophys.*, 23, 733.

Chisham, G., M. P. Freeman, M. M. Lam, G. A. Abel, T. Sotirelis, R. A. Greenwald, and M. Lester (2005b), A statistical comparison of Super-DARN spectral width boundaries and DMSP particle precipitation boundaries in the afternoon sector ionosphere, *Ann. Geophys.*, 23, 3645.

Eriksson, P. T. I., L. G. Blomberg, A. D. M. Walker, and K. H. Glassmeier (2005), Poloidal ULF oscillations in the dayside magnetosphere: A Cluster study, *Ann. Geophys.*, 23, 2679–2686, doi:10.5194/angeo-23-2679-2005.

Friedberg, W., K. Copeland, F. E. Duke, K. O'Brien, and E. B. Darden Jr. (2000), Radiation exposure during air travel: Guidance provided by the Federal Aviation Administration for air carrier crews, *Health Phys.*, 79(5), 115–134.

Gerrard, A. J., D. Detrick, S. B. Mende, L. J. Lanzerotti, A. T. Weatherwax, and Y. Bhattacharya (2010), Photometric observations of 630.0-nm OI and 427.8-nm N2+ emission from South Pole and McMurdo Stations during winter: Analysis of temporal variations spanning minutes to hourly timescales, *J. Geophys. Res.*, 115, A08231, doi:10.1029/2009JA014970.

Gombosi, T. I., K. G. Powell, D. L. D. Zeeuw, C. R. Clauer, K. C. Hansen, W. B. Manchester, A. J. Ridley, I. I. Roussev, V. Sokolov, and Q. F. Stout (2004), Solution-adaptive magnetohydrodynamics for space plasmas: Sun-to-earth simulations, *Comp. Sci. Eng.*, 6(2), 14–35, doi:10.1109/MCISE.2004.1267603.

Holzworth, R. H., and C. Meng (1975), Mathematical representation of the auroral oval, *Geophys. Res. Lett.*, 2(9), 377–380, doi:10.1029/GL002i009p00377.

Jones, J. B. L., R. D. Bentley, R. Hunter, R. H. A. Iles, G. C. Taylor, and D. J. Thomas (2004), On space weather consequences and predictions, *Adv. Space Res.*, 36(12), 2258–2267.

Kamide, Y., S. Kokubun, L. F. Bargatze, and L. A. Frank (1999), The size of the polar cap as an indicator of substorm energy, *Phys. Chem. Earth*, 24(1–3), 119–127.

Kepko, L., H. E. Spence, and H. J. Singer (2002), ULF waves in the solar wind as direct drivers of magnetospheric pulsations, *Geophys. Res. Lett.*, 29(8), 1197, doi:10.1029/2001GL014405.

Lanzerotti, L. J., A. Shono, H. Fukunishi, and C. G. Maclennan (1999), Long-period hydromagnetic waves at very high geomagnetic latitudes, *J. Geophys. Res.*, 104(A12), 28,423–28,435.

Lessard, M. R., et al. (2009), PENGUIn multi-instrument observations of dayside high-latitude injections during the 23 March 2007 substorm, *J. Geophys. Res.*, 114, A00C11, doi:10.1029/2008JA013507. [Printed 155(A1), 2010.]

Liou, K., K. Takahashi, P. T. Newell, and K. Yumoto (2008), Polar ultraviolet imager observations of solar wind–driven ULF auroral pulsations, *Geophys. Res. Lett.*, 35, L16101, doi:10.1029/2008GL034953.

Lockwood, M., J. Moen, A. P. van Eyken, J. A. Davies, K. Oksavik, I. W. McCrea, and M. Lester (2005), Motion of the dayside polar cap boundary during substorm cycles: I. Observations of pulses in the magnetopause reconnection rate, *Ann. Geophys.*, 23(11), 3495–3511.

Mende, S. B., et al. (2009), Observations of earth space by self-powered stations in Antarctica, *Rev. Sci. Instrum.*, 80(12), 124501, doi:10.1063/1.3262506.

Milan, S. E. (2004), A simple model of the flux content of the distant magnetotail, *J. Geophys. Res.*, 109, A07210, doi:10.1029/2004JA010397.

Milan, S. E., M. Lester, S. W. H. Cowley, K. Oksavik, M. Brittnacher, R. A. Greenwald, G. Sofko, and J. P. Villain (2003), Variations in the polar cap area during two substorm cycles, *Ann. Geophys.*, 21(5), 1121–1140.

Milan, S., J. Wild, A. Grocott, and N. Draper (2006), Space- and ground-based investigations of solar wind-magnetosphere-ionosphere coupling, *Adv. Space Res.*, 38(8), 1671–1677, doi:10.1016/j.asr.2005.08.009.

Moen, J., M. Lockwood, K. Oksavik, H. C. Carlson, W. F. Denig, A. P. van Eyken, and I. W. McCrea (2004), The dynamics and relationships of precipitation, temperature and convection boundaries in the dayside auroral ionosphere, *Ann. Geophys.*, 22, 1973–1987.

Oksavik, K., F. Soraas, J. Moen, and W. J. Burke (2000), Optical and particle signatures of magnetospheric boundary layers near magnetic noon: Satellite and ground-based observations, *J. Geophys. Res.*, 105(A12), 27,555–27,568.

Patterson, J. D., T. P. Armstrong, C. M. Laird, D. L. Detrick, and A. T. Weatherwax (2001), Correlation of solar energetic protons and polar cap absorption, *J. Geophys. Res.*, 106(A1), 149–163.

Pulkkinen, T. I., and N. A. Tsyganenko (1996), Testing the accuracy of magnetospheric model field line mapping, *J. Geophys. Res.*, 101(A12), 27,431–27,442.

Rae, I. J., K. Kabin, R. Rankin, F. R. Fenrich, W. Liu, J. A. Wanliss, A. J. Ridley, T. I. Gombosi, and D. L. De Zeeuw (2004), Comparison of photometer and global MHD determination of the open-closed field line boundary, *J. Geophys. Res.*, 109, A01204, doi:10.1029/2003JA009968.

Ridley, A. J., T. I. Gombosi, and D. L. De Zeeuw (2004), Ionospheric control of the magnetospheric configuration: Conductance, *Ann. Geophys.*, 22, 567–584.

Riley, P. (2007), Modeling corotating interaction regions: From the Sun to 1 AU, *J. Atmos. Sol. Terr. Phys.*, 69(1–2), 32–42.

Rodger, A. S. (2000), Ground-based imaging of magnetospheric boundaries, *Adv. Space Res.*, 25(7–8), 1461–1470.

Rose, D. C., and S. Ziauddin (1962), The polar cap absorption effect, *Space Sci. Rev.*, 1(1), 115–134.

Rosenberg, T. J., and J. H. Doolittle (1994), Studying the polar ionosphere and magnetosphere with automatic geophysical observatories: The U. S. program in Antarctica, *Antarct. J. U. S.*, 29(5), 347.

Shea, M. A., and D. F. Smart (1998), Space weather: The effects on operations in space, *Adv. Space Res.*, 22(1), 29–38.

Siscoe, G. L., and T. S. Huang (1985), Polar cap inflation and deflation, *J. Geophys. Res.*, 90(A1), 543–547.

Sotirelis, T., P. T. Newell, C.-I. Meng, and G. L. Siscoe (1998), Shape of the open-closed boundary of the polar cap as determined from observations of precipitating particles by up to four DMSP satellites, *J. Geophys. Res.*, 103, 399–406, doi:10.1029/97JA02437.

Thomson, D. J., C. G. Maclennan, and L. J. Lanzerotti (1995), Propagation of solar oscillations through the interplanetary medium, *Nature*, 376, 139–144, doi:10.1038/376139a0.

Toth, G. V., et al. (2005), A physics-based software framework for sun-earth connection modeling, in *Multiscale Coupling of Sun-Earth Processes*, edited by A. T. Y. Liu, Y. Kamide, and G. Consolini, pp. 383–397, Elsevier, New York.

Tsurutani, B. T., et al. (2006), Corotating solar wind streams and recurrent geomagnetic activity: A review, *J. Geophys. Res.*, 111, A07S01, doi:10.1029/2005JA011273.

Tsyganenko, N. A. (1995), Modeling the Earth's magnetospheric field confined within a realistic magnetopause, *J. Geophys. Res.*, 100(A4), 5599–5612.

Tsyganenko, N. A., and M. I. Sitnov (2007), Magnetospheric configurations from a high-resolution data-based magnetic field model, *J. Geophys. Res.*, 112, A06225, doi:10.1029/2007JA012260.

Y. Bhattacharya, A. J. Gerrard, L. J. Lanzerotti, and K. D. Urban, Center for Solar-Terrestrial Research, New Jersey Institute of Technology, 323 Martin Luther King Blvd., 101 Tiernan Hall, Newark, NJ 07102-1982, USA. (andres.j.gerrard@njit.edu)

A. J. Ridley, University of Michigan, 1416 Space Research Bldg., Ann Arbor, MI 48109-2143, USA. (ridley@umich.edu)

A. T. Weatherwax, Department of Physics, Siena College, Loudonville, NY 12211-1462, USA. (aweatherwax@siena.edu)